Electronic Supplementary Material (ESI) for Energy & Environmental Science.

Supporting Information

Amorphous S-rich $S_{1-x}Se_x$/C (x≤0.1) Composites Promise Better Lithium Sulfur Batteries in Carbonate-based Electrolyte

Xiaona Li, Jianwen Liang, Kailong Zhang, Zhiguo Hou, Wanqun Zhang, *Yongchun Zhu,** and Yitai Qian*

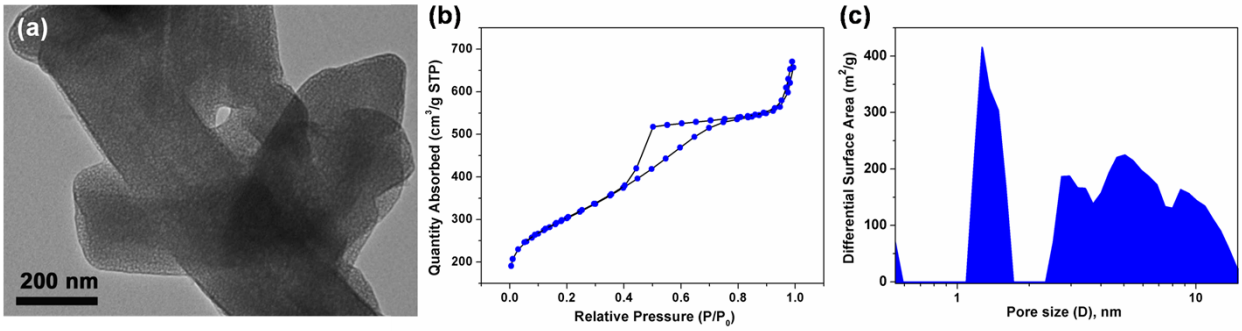

Figure S1. (a) TEM image, (b) nitrogen sorption isotherms, and (c) pore size distributions of the as-prepared porous carbon.

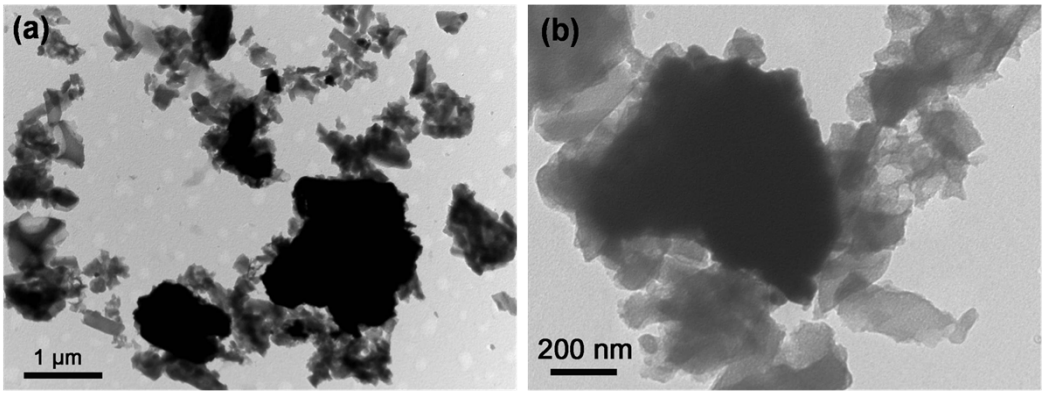

Figure S2. (a,b) TEM images of the mixture of Se, S and porous carbon after the ball-milled process.

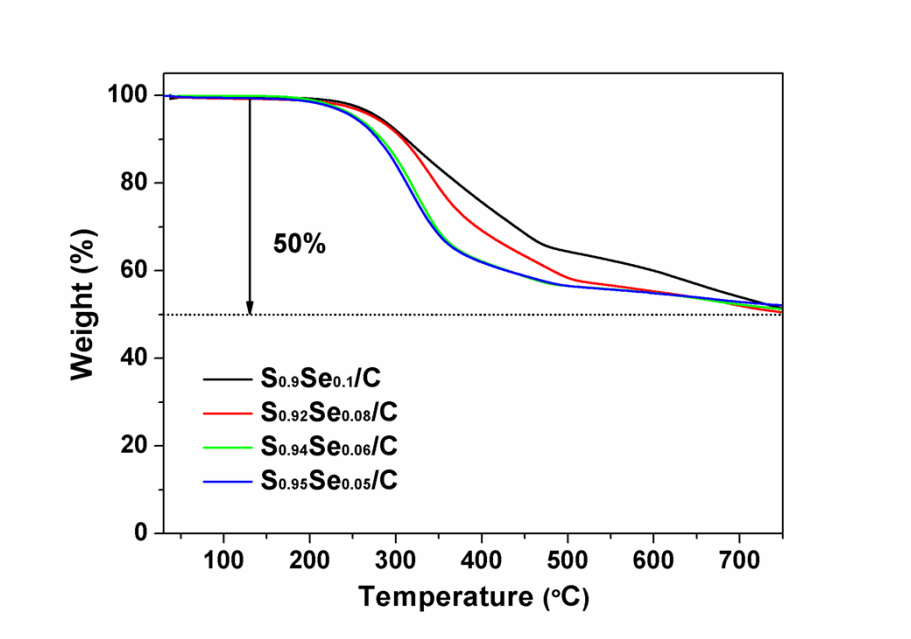

Figure S3. Thermogravimetric analysis of the as-prepared $S_{1-x}Se_x/C$ composites. All the tests were conducted with a temperature ramp of 10 °C min^{-1} in N_2.

Table S1. The Se, S and C content in the $S_{1-x}Se_x/C$ samples (x=0.05, 0.06, 0.08, 0.1) based on thermogravimetric analysis and elemental analysis.

Statement	Se (wt%)	S (wt%)	C (wt%)	x in $S_{1-x}Se_x/C$
$S_{0.9}Se_{0.1}/C$	10.9	38.9	50.2	0.102
$S_{0.92}Se_{0.08}/C$	8.65	41.05	50.3	0.079
$S_{0.94}Se_{0.06}/C$	7.4	42.9	49.7	0.065
$S_{0.95}Se_{0.05}/C$	6.4	45.3	48.3	0.054

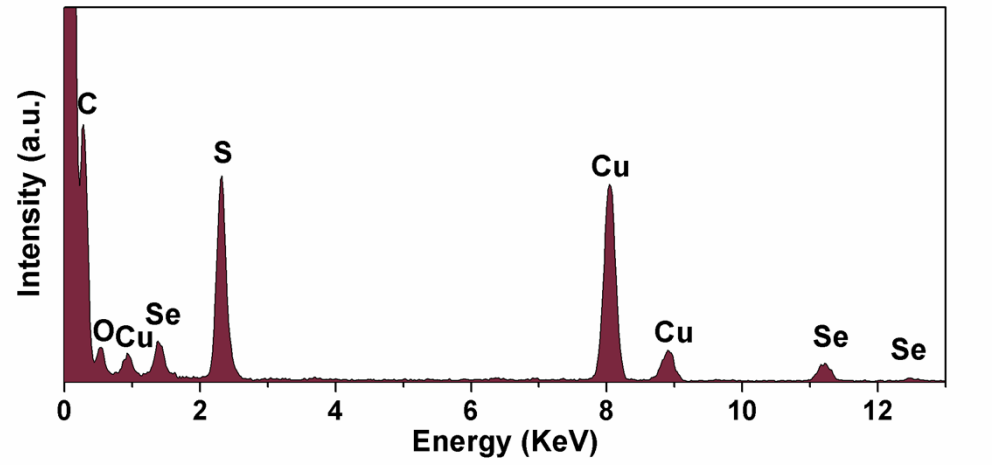

Figure S4. EDS spectrum of the $S_{0.94}Se_{0.06}/C$ sample.

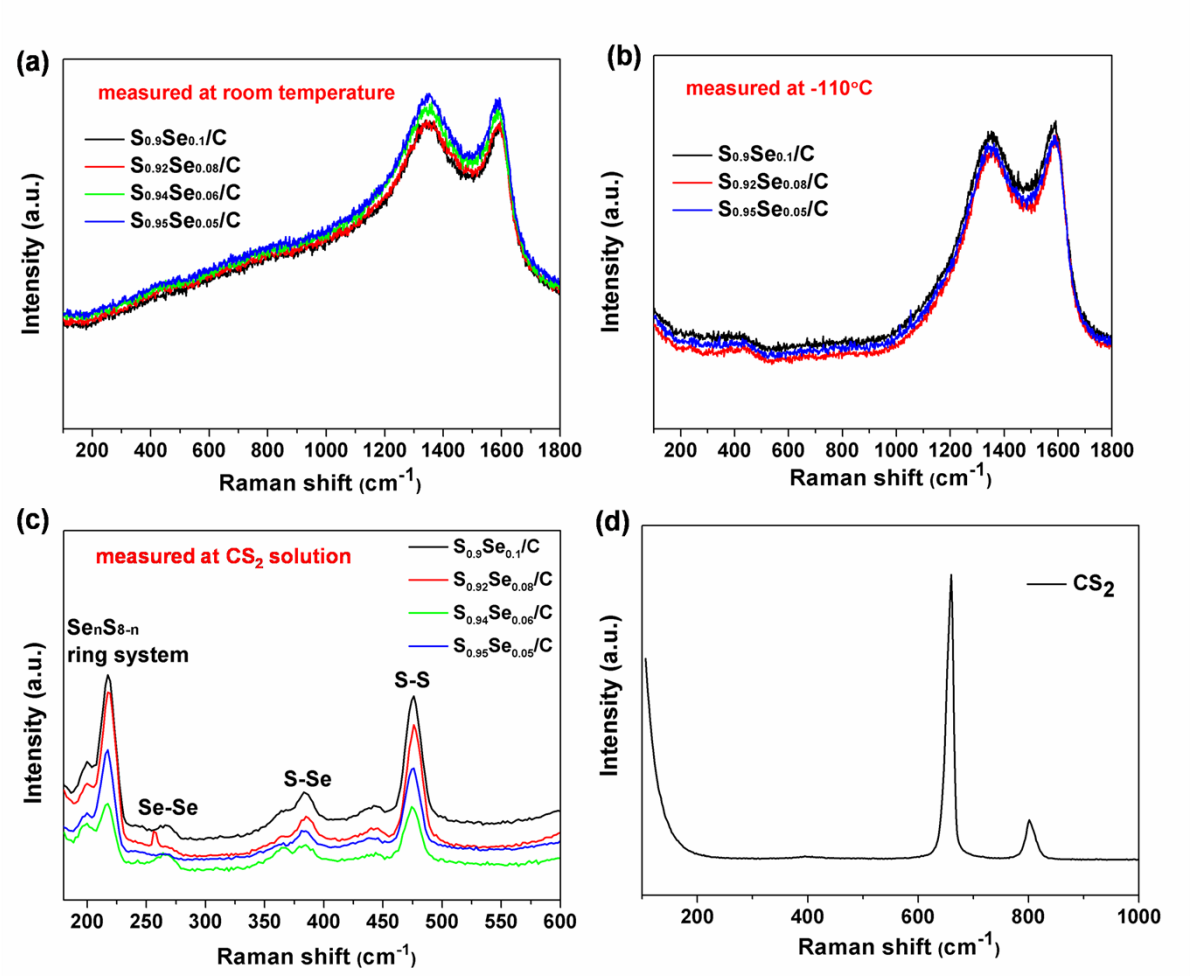

Figure S5. (a) Raman spectra of $S_{1-x}Se_x/C$ samples recorded at room temperature, (b) Raman spectra of $S_{1-x}Se_x/C$ samples (x=0.05, 0.08, 0.1) recorded at -110 °C. (c) Raman spectra of $S_{1-x}Se_x/C$ samples in CS_2 solution, (d) Raman spectrum of CS_2 solution.

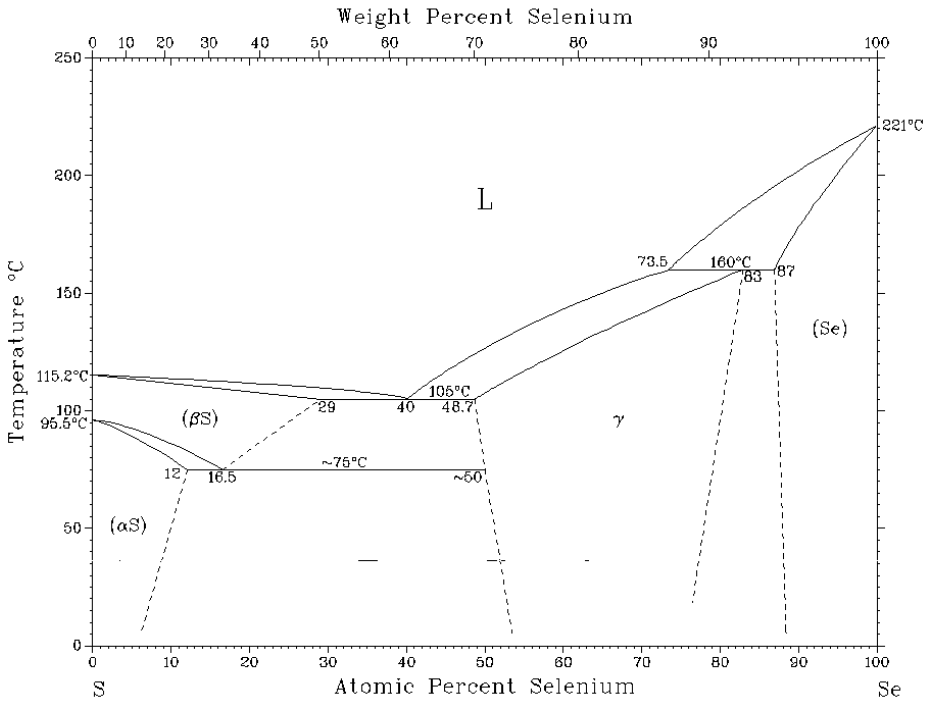

Figure S6. The phase diagram of sulphur-selenium binary system.

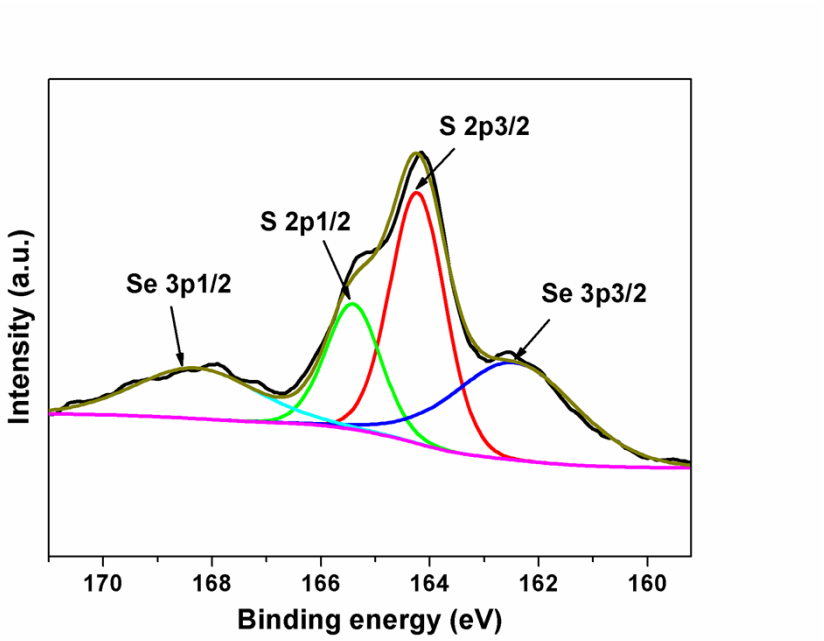

Figure S7. XPS spectra of S 2p and Se 3p in the $S_{0.94}Se_{0.06}$ sample without carbon after heat treatment.

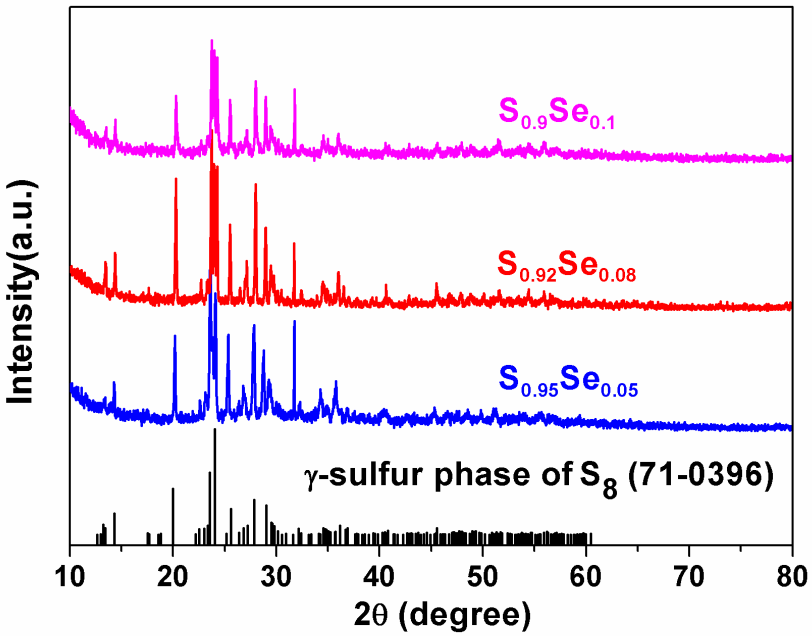

Figure S8. XRD patterns of $S_{0.9}Se_{0.1}$, $S_{0.92}Se_{0.08}$ and $S_{0.95}Se_{0.05}$ samples without carbon after heat treatment.

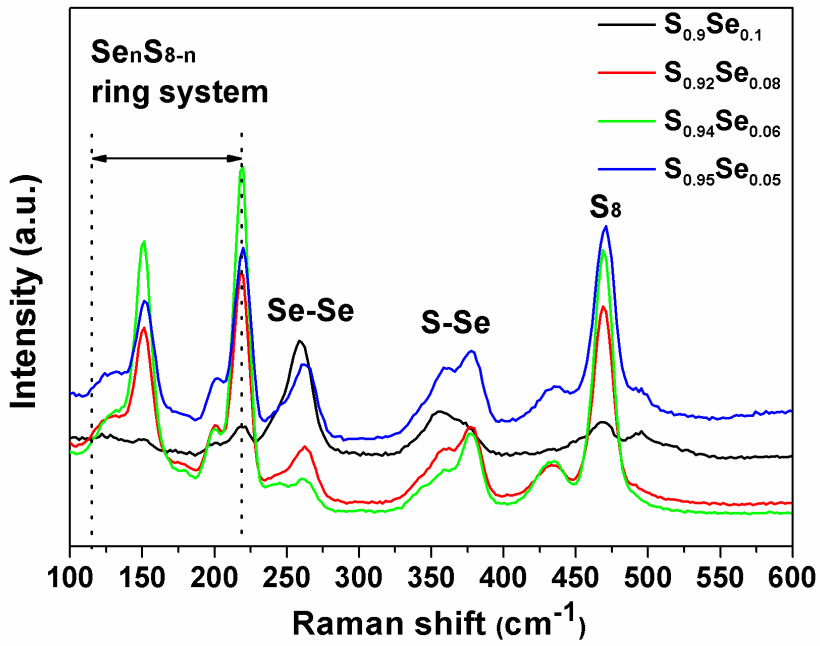

Figure S9. Raman spectra of $S_{1-x}Se_x$ (x = 0.05, 0.06, 0.08, 0.1) samples recorded at room temperature.

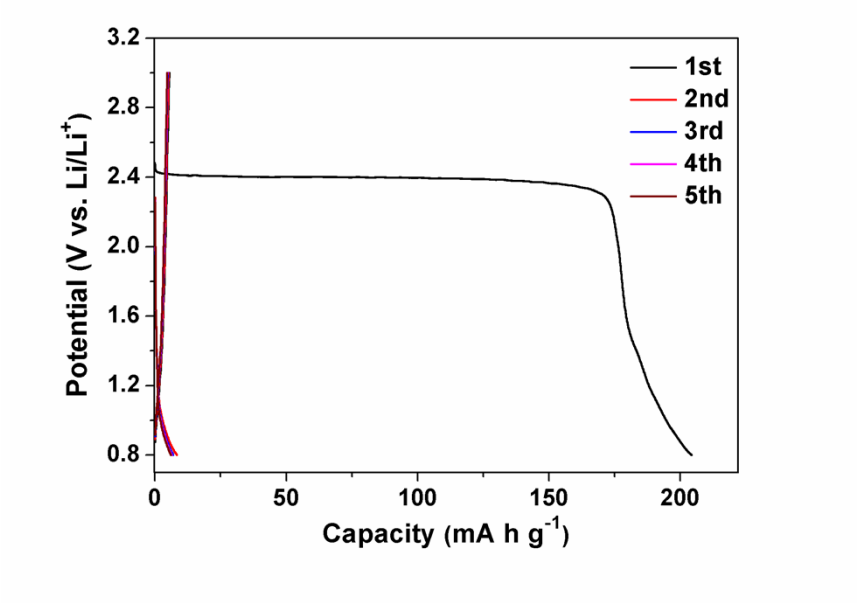

Figure R10. Typical galvanastatic discharge-charge curves of the cell with $S_{0.94}Se_{0.06}$ in the potential region of 0.8–3 V versus Li/Li^+ at 0.02 A g^{-1}.

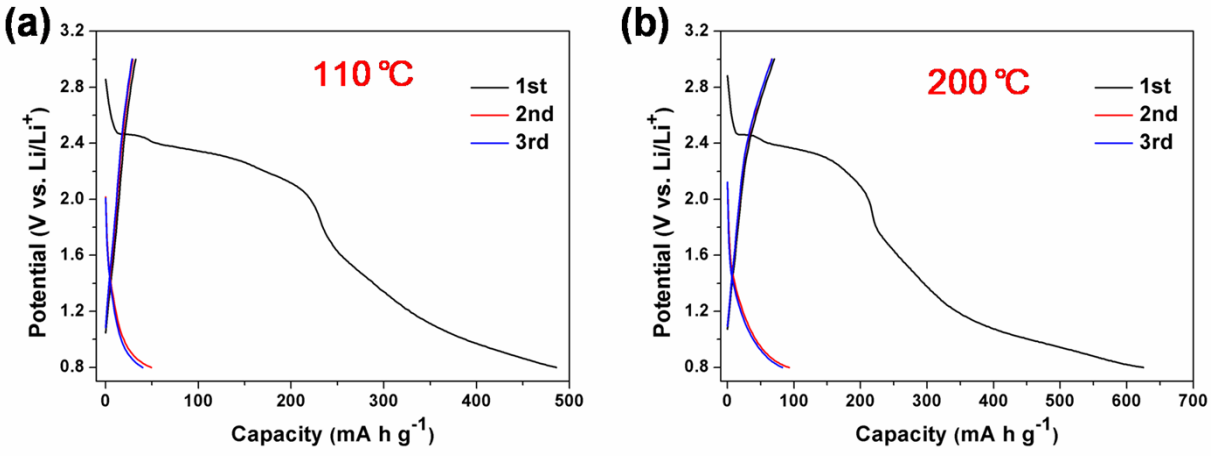

Figure S11. Discharge/charge profiles of $S_{0.94}Se_{0.06}$/C samples obtained at 110 and 200 °C, respectively, with current density of 0.2 A g^{-1}.

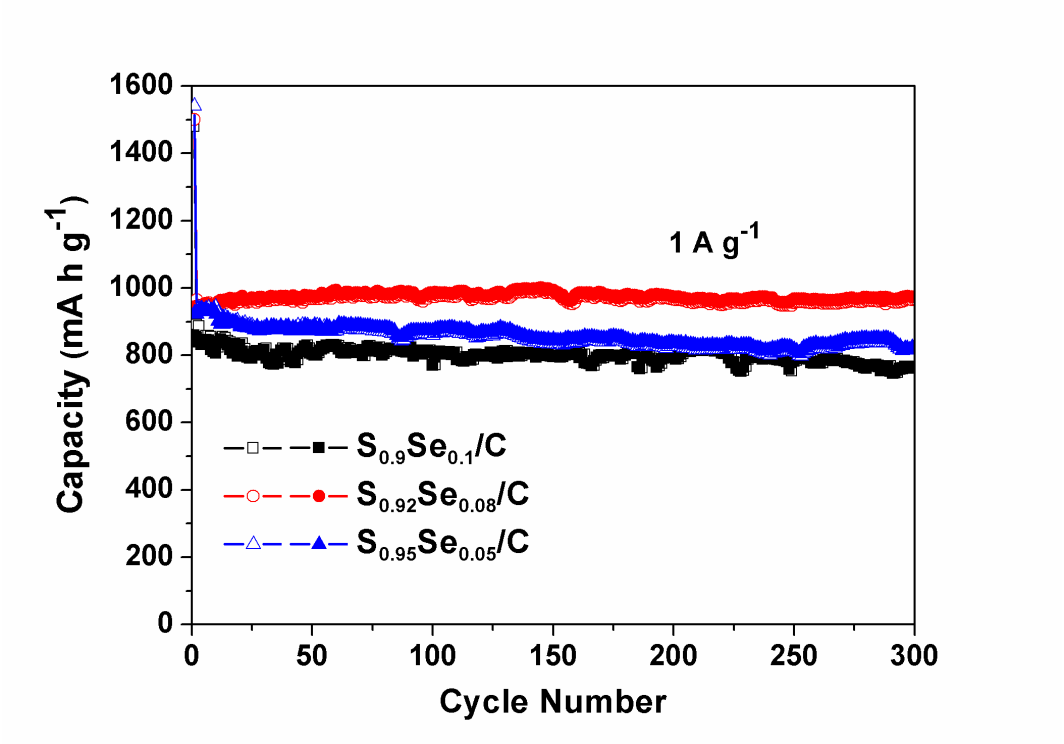

Figure S12. Cycling performance of $S_{1-x}Se_x/C$ samples (x=0.05, 0.08, 0.1) at 1 A g^{-1}.

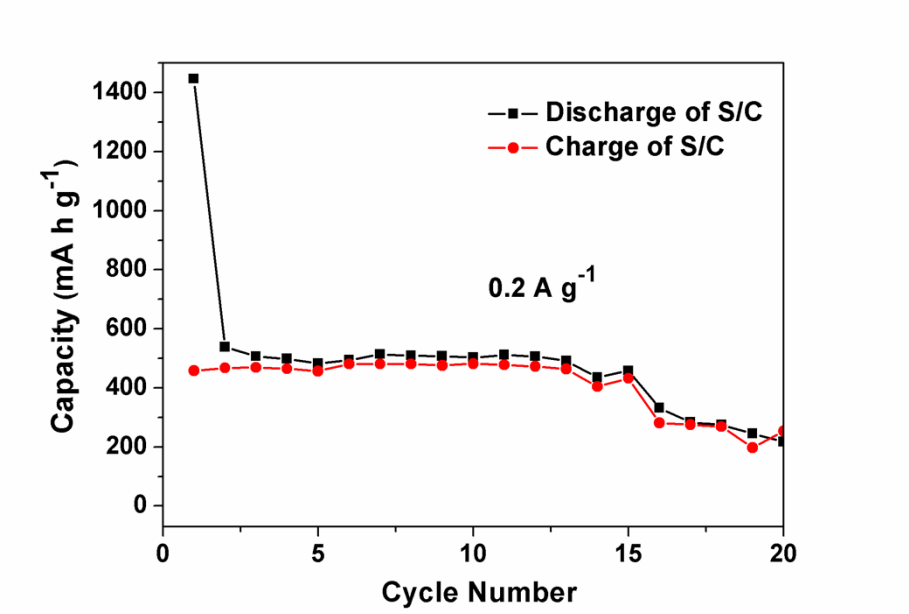

Figure S13. Cycling performance of S/C composites at 0.2 A g^{-1}.

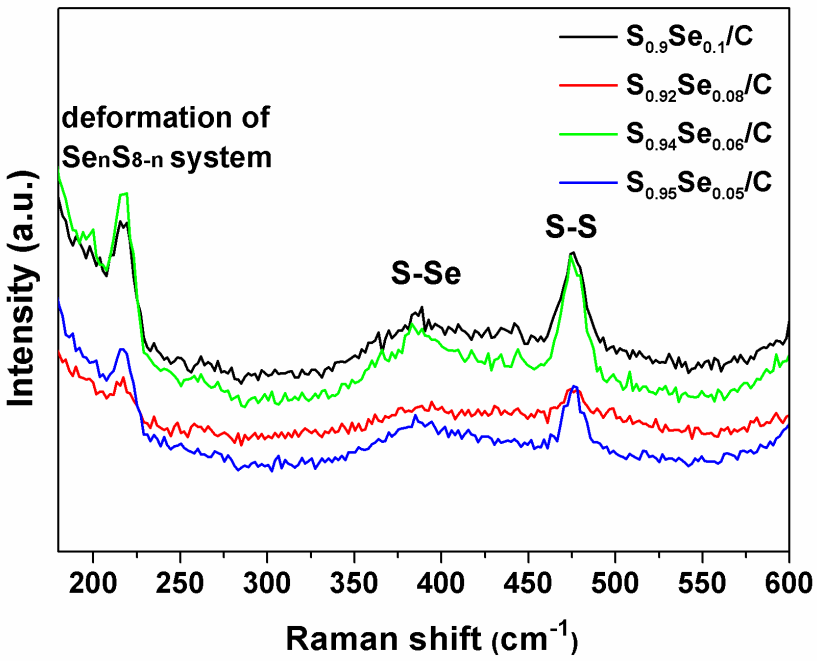

Figure S14. Raman spectra of $S_{1-x}Se_x$/C electrodes at charge state recorded in CS_2 solution.

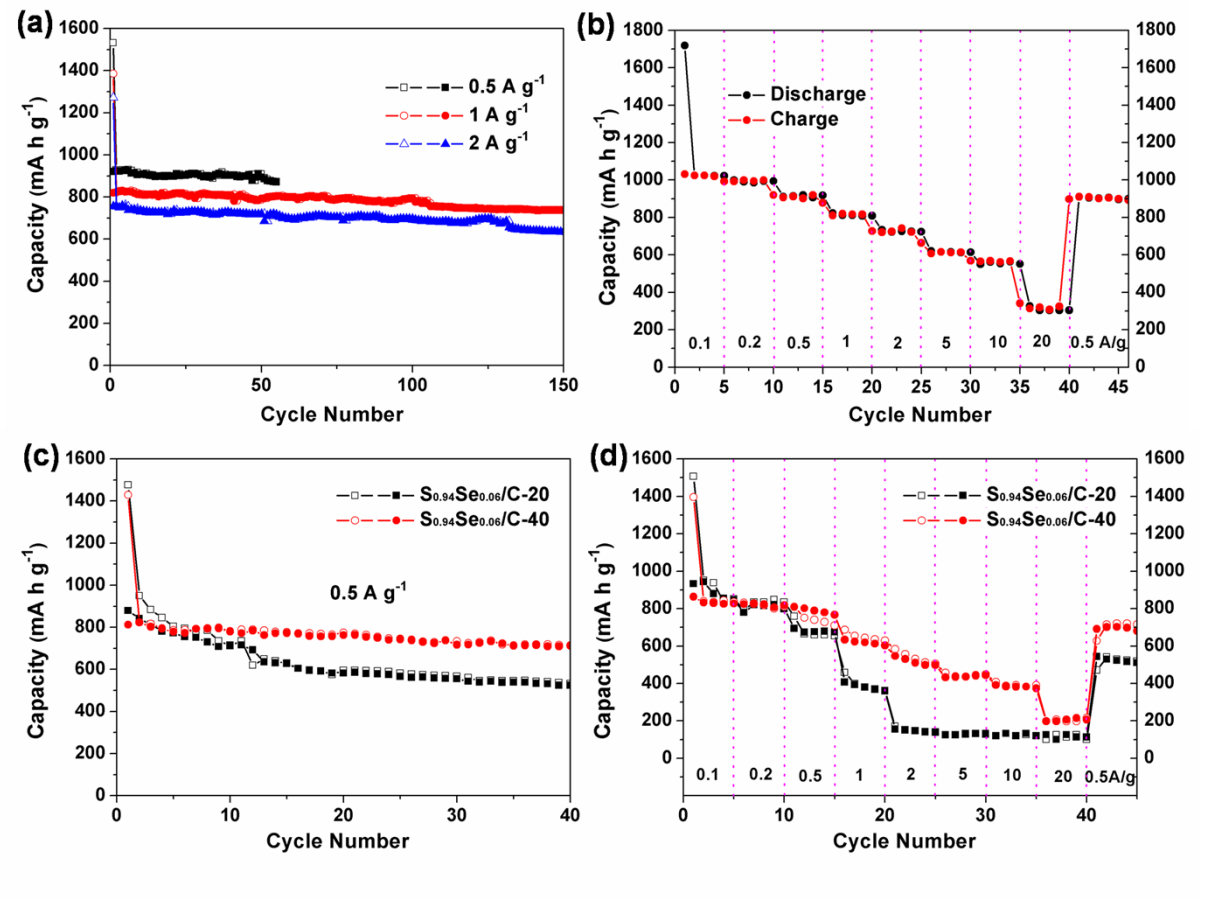

Figure R15. (a) Cycling performance of $S_{0.94}Se_{0.06}$/C electrode with higher loading about 2-3 mg cm^{-2} at current density of 0.5, 1 and 2 A g^{-1}. (b) Cycle performance of $S_{0.94}Se_{0.06}$/C electrode with higher loading about 2-3 mg cm^{-2} at various current rates: 0.1, 0.2, 0.5, 1, 2, 5, 10, and 20 A g^{-1} and then back to 0.5 A g^{-1}. (c) Cycling performance of $S_{0.94}Se_{0.06}$/C-20 and $S_{0.94}Se_{0.06}$/C-40 electrodes at current density of 0.5 A g^{-1}. (d) Cycle performance of $S_{0.94}Se_{0.06}$/C-20 and $S_{0.94}Se_{0.06}$/C-40 electrodes at various current rates: 0.1, 0.2, 0.5, 1, 2, 5, 10, and 20 A g^{-1} and then back to 0.5 A g^{-1}.

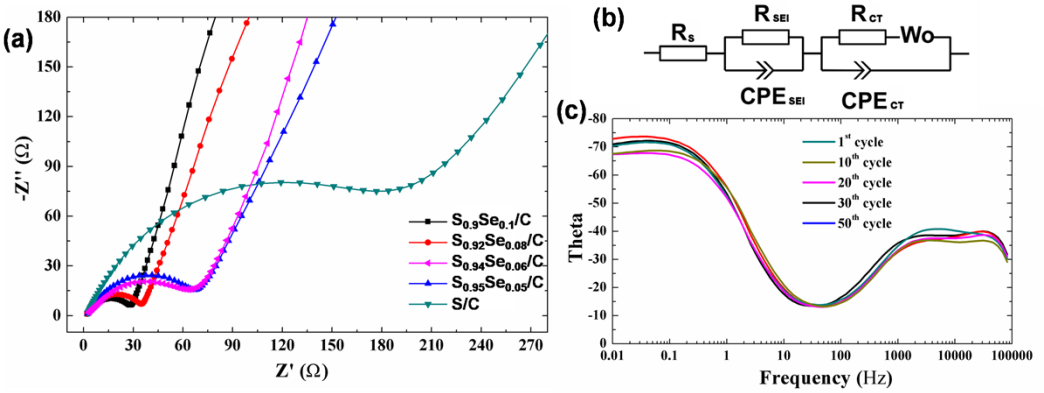

Figure S16. (a) The electrochemical impedance spectra of the different $S_{1-x}Se_x/C$ samples (x=0.05, 0.06, 0.08, 0.1) and S/C composite cathodes (the scattered data points and continuous lines represent experimental data and corresponding fitting results, respectively). (b) The corresponding equivalent circuits. The impedance of different $S_{1-x}Se_x/C$ (x=0.05, 0.06, 0.08, 0.1) electrodes are measured by alternating current (AC) impedance spectroscopy in their full charge state after 1 cycle (Figure S13a). All of the impedance diagrams consist of a large-radius semicircle in the high-frequency region and inclined line in the low-frequency region. Although complex impedance plot looks to give single semicircle, it has two relaxation processes in the high-frequency region. The complex modulus plots (Figure S13c) make these clear, giving two distinct semicircles in high-frequency region. Due to the cell is combined with solid electrode and electrolyte, one is attributed to the surface SEI layers (R_{SEI}) and the other to the charge transfer in electrode material (R_{ct}). Thus, all EIS plots are fitted with equivalent circuits by series of R (electrolyte resistance, R_s) and two parallel RC circuits (Figure S13b). The obtained results are shown in Table S2 in the Supporting Information. As shown in Table S2, the $S_{0.95}Se_{0.05}/C$ composite cathode demonstrated the highest R_{ct} which means the highest resistance compared with other three electrodes. Moreover, the electrical conductivity of the $S_{1-x}Se_x/C$ composite cathodes increases significantly along with the increase of the content of Se.

Table S2. Equivalent-circuit parameters obtained from fitting the experimental impedance spectra.

Statement	$R_s(\Omega)$	$R_{SEI}(\Omega)$	$R_{CT}(\Omega)$	$CPE_{SEI}(F)$ [a)]	$CPE_{CT}(F)$ [a)]
S/C	2.39	3.00	172.8	3.28E-6	1.15E-5
$S_{0.95}Se_{0.05}/C$	2.44	1.02	67.54	1.16 E-7	6.27 E-5
$S_{0.94}Se_{0.06}/C$	2.43	2.52	60.1	7.93E-7	1.50E-5
$S_{0.92}Se_{0.08}/C$	2.03	3.49	27.06	4.52 E-6	1.22 E-5
$S_{0.90}Se_{0.1}/C$	2.04	2.72	21.96	4.03 E-6	1.35 E-5

[a)] CPE_1 and CPE_2: represent the two resistors with constant phase elements.

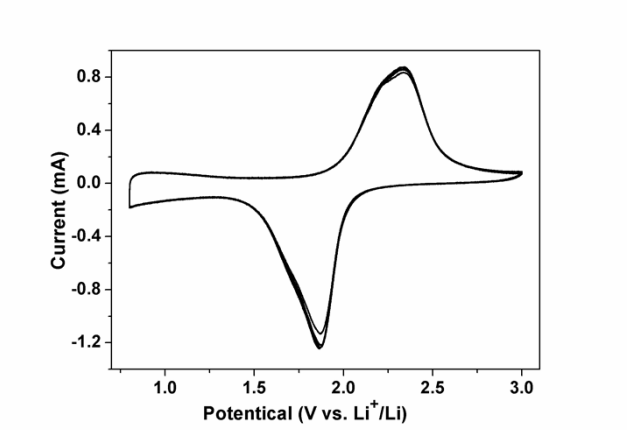

Figure S17. CV curves for $S_{0.94}Se_{0.06}$/C electrode at a scan rate of 0.1 mV s^{-1} in the voltage range of 3.0–0.8 V vs Li^+/Li after 300 cycles test.

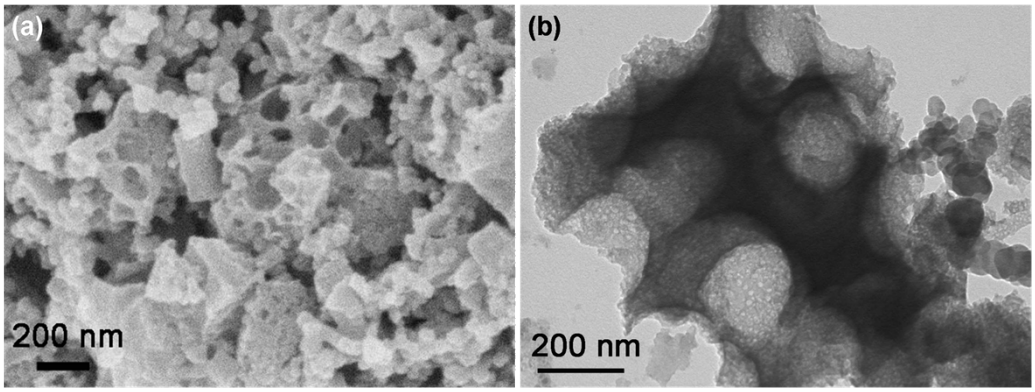

Figure S18. (a) SEM and (b) TEM images of the $S_{0.94}Se_{0.06}$/C electrode after 500 cycles.